Int. J. Multiphase Flow Vol. 18, No. 6, pp. 905–926, 1992
Printed in Great Britain.

0301-9322/92 $5.00 + 0.00

MODELLING OF PARTICLE–WALL COLLISIONS IN CONFINED GAS–PARTICLE FLOWS

M. SOMMERFELD
Lehrstuhl für Strömungsmechanik, Universität Erlangen/Nürnberg, Cauerstr. 4, 8520 Erlangen, Germany

(Received 5 December 1990; in revised form 25 August 1992)

Abstract—This paper demonstrates that numerical simulations of confined particulate two-phase flows require a detailed modelling of particle–wall collisions which includes the wall surface structure and the particle shape. These effects are taken into account by "irregular bouncing" models which are based on the statistical treatment of the collision process. In this study, results obtained using various "irregular bouncing" models based on the impulse equations for a particle–wall collision are considered and compared with experimental observations. The wall roughness is simulated by assuming that the particle collides with a virtual wall which has a randomly distributed inclination with respect to the plane, smooth wall. A Gaussian distribution for this random inclination showed the best agreement with experimental results. Numerical predictions of a turbulent two-phase flow in a vertical channel, where the particle phase is treated using a Lagrangian approach, showed that the different models applied for a particle–wall collision have a strong effect on the particle velocity fluctuations and the mass flux profiles in the region of fully developed flow. The numerical simulations using the irregular bouncing models yielded considerably higher values for the particle velocity fluctuations, which also agreed better with the experimental values. This effect was most pronounced for large particles, where the distance they need to respond to the fluid flow is larger than the characteristic dimension of the confinement. On the other hand, the motion of small particles is less affected by the choice of the wall-collision model. These effects of the wall roughness on the velocity fluctuations of the dispersed phase have not been considered in previous studies using irregular bouncing models.

Key Words: gas–particle flow, particle–wall collision, wall roughness, numerical predictions

1. INTRODUCTION

In many practical situations, particulate two-phase flows are confined, turbulent flows, e.g. in pneumatic conveying lines or cyclone separators. The confinement may considerably influence the particle motion and hence the velocity statistics as a result of particle–wall collisions. Therefore, it is necessary to apply detailed physical models for the particle bouncing process on the wall in numerical simulations of such flows. For dilute two-phase flows, two characteristic regimes of particle behaviour with regard to the importance of particle–wall collisions may be distinguished based on the particle size or the particle response time:

- The motion of relatively small particles is controlled by fluid motion and turbulent dispersion. The influence of the particle–wall bouncing is less important since the particles promptly follow the carrier fluid after a collision. For such situations, the numerical simulation of the particle interaction with the mean flow and the fluid turbulence has been improved to a large extent so that good agreement with experimental data could be achieved (Gosman & Ioannides 1983; Elghobashi & Abou-Arab 1983; Shuen *et al.* 1985; Milojevic *et al.* 1986; Sommerfeld & Zeisel 1988; Berlemont *et al.* 1990).
- In the case of large particles, their motion is dominated by inertia and not strongly influenced by flow turbulence. Such large particles also respond slowly to changes in the mean flow, so that their motion may be considerably influenced by the wall-collision process in confined flows, such as after particle injection facilities in pipe bends or branches. Due to their inertia, the particles maintain their direction of motion for a long time after they rebound off a wall, which results in the next collision with the opposite wall.

An estimate of the particle size, for which wall collisions dominate the particle motion, may be based on the Stokesian time constant and the distance required for a particle to reach the wall. For a vertical plane channel flow, where the particles disperse from a line source with a certain ratio of transverse velocity fluctuation (RMS) to the mean streamwise velocity, a collision-dominated two-phase flow may be defined when more than 30% of the particles collide with the wall before these respond to the fluid flow. The particle relaxation length (λ_p) is obtained by multiplying the Stokesian particle response time by the average streamwise particle velocity at the line source:

$$\lambda_p = \frac{\rho_p D_p^2}{18\mu} \overline{u_p},$$

where ρ_p is the particle density, D_p is the particle diameter, μ is the dynamic viscosity and $\overline{u_p}$ is the averaged axial particle mean velocity. The maximum lateral distance (L) for which 30% of the particles starting from the line source collided with a wall is

$$L = \frac{\overline{u_p}}{0.7 v_p'} D,$$

where D is the width of the channel, v_p' is the transverse velocity fluctuation which is assumed to have a constant probability distribution. Assuming that v_p' may be expressed as a fraction K of $\overline{u_p}$ ($v_p' = K\overline{u_p}$), the particle diameter for which a two-phase flow is dominated by wall collisions is given by

$$D_p > \sqrt{\frac{18\mu D}{0.7\, K\, \overline{u_p} \rho_p}}.$$

This diameter, defining a wall-collision-dominated two-phase flow, is given in table 1 for different transverse velocity fluctuations and channel widths for glass beads ($\rho_p = 2.5$ g/cm^3) with a mean streamwise velocity of $\overline{u_p} = 10$ m/s in air ($\mu = 18.5\, 10^{-6}$ N s/m^2). The minimum particle size for which the particle motion is strongly determined by wall collisions decreases with increasing transverse velocity fluctuations and increases with the channel width, since the particles have more time to respond to the fluid flow.

There is still too little experimental information for wall-collision-dominated particulate two-phase flows to allow a detailed modelling of a particle–wall collision and subsequently realistic numerical simulations. This is not surprising, since a large number of parameters affect a particle–wall collision. Some of the most important parameters are listed below:

- Particle collision angle.
- Particle translational and rotational velocities before collision.
- Properties of the particle and wall materials.
- Particle shape and roughness of the wall surface.

Aerodynamic effects during the collision process (i.e. the displacement of the air between the particle and wall) can be neglected for gas–solid flows since the particle Reynolds number is >1 (Durst & Raszillier 1989). The fact that a large number of parameters can affect particle–wall collisions may account for the large scatter of experimental data for the restitution and friction coefficients (Brauer 1980; Yamamoto 1986; Govan *et al.* 1989). These values characterize the velocity change during a collision process and are needed as input to the numerical model.

In a number of experiments performed by Brauer (1980) for different collision angles, it was shown that the coefficient of restitution as well as the difference between the collision and reflection angles strongly depend on the material properties of the wall and the particles. In these experiments,

Table 1. Minimum particle diameter for wall-collision-dominated gas–particle flow

	D_p (μm)	
D (mm)	$K = 0.05$	$K = 0.1$
25	69	98
50	98	138
100	138	195

a 6 mm steel ball was used in combination with several target materials. For a target material consisting of PMMA, for example, a normal coefficient of restitution of 0.93 was obtained for collision angles $>30°$, whereas between 0° and 30°, an almost linear decrease from 1.0 to 0.93 was observed. These results, however, have only a limited application to real situations, since the wall roughness will not considerably affect the collision process for such large particles.

In experiments performed by Yamamoto (1986), who studied the collision of a 3 mm polyethylene sphere with a flat plate, an almost constant coefficient of restitution of 0.92 (with some scatter) for different collision angles was obtained.

In a recent work by Govan *et al.* (1989), the bouncing characteristics of resin and glass particles (particle dia $D_p = 600$ and 550 μm, respectively) on a copper plate were studied. The results showed that the total coefficient of restitution decreases with increasing collision angle (i.e. from 0.85 at 10° to about 0.7 at 30°). These data, however, are scattered in a rather broad band which was also observed for the difference between the collision and reflection angles.

In connection with the erosion of turbine blades, Tabakoff and co-authors (Grant & Tabakoff 1975; Tabakoff & Hamed 1977) performed a large number of experimental studies on particle–wall collisions and derived several particle rebound correlations for different material combinations, e.g. aluminium alloy and quartz sand ($D_p = 200$ μm). In the results of Grant & Tabakoff (1975), a large scatter in the particle velocities after collision and the reflection angle is obtained, which is most likely due to irregularities in the particle shape and the roughness of the target material. To characterize the bouncing process, correlations are given for the mean values and the standard deviations of the velocity restitution coefficients and the reflection angle as a function of the particle collision angle (Tabakoff & Hamed 1977). These correlations in connection with a statistical procedure are, furthermore, used to numerically simulate particle–wall collisions and the associated erosion rates (Grant & Tabakoff 1975).

Due to the limited experimental information available on the details of a particle–wall collision and the different situations in two-phase flows (e.g. the material of the particle and the wall, particle shape and wall roughness) it is difficult to establish a generally applicable particle–wall collision model for the numerical simulations of particulate two-phase flows. The considerable influence of the wall-collision model on the numerically simulated particle concentration distributions in horizontal pneumatic conveying has been demonstrated previously in several publications (Matsumoto & Saito 1970a, b; Tsuji *et al.* 1985). Recently, Sommerfeld (1990a) emphasized the importance of particle–wall collision modelling on the numerically predicted velocity characteristics of the particle phase (i.e. particle velocity fluctuations) in a vertical plane channel flow.

2. MODELS FOR SIMULATING PARTICLE–WALL COLLISIONS

In numerical simulations of turbulent particulate two-phase flows, using the Lagrangian approach for the particle phase, particle–wall collisions are usually treated as ideal reflections without any loss of particle momentum (e.g. Shuen *et al.* 1985; Milojevic *et al.* 1986). This procedure may be valid for two-phase flows, where the particles are small enough to follow the mean flow and the turbulent velocity fluctuations to a large extent. Even though the particle loses some momentum during a wall-collision process and will rebound in different directions due to the surface roughness, it will be quickly accelerated to its original velocity and entrained by the gas flow.

For large particles in a confined flow situation, as defined above, the particle motion is controlled by wall collisions and a detailed modelling of the collision process is necessary to simulate the particle properties realistically.

An appropriate particle–wall collision model may be either purely empirical (e.g. Grant & Tabakoff 1975) or based on the impulse equations for the collision of a particle with a wall (Matsumoto & Saito 1970b; Tsuji *et al.* 1985; Oesterle 1989). Since the first approach requires a large number of experiments and is not universally applicable, the second approach was preferred for the present study. The particle translational and rotational velocities after a wall collision may be derived from the impulsive equations for a particle–wall collision, where two types of collision

are distinguished: a collision with and without sliding (Matsumoto & Saito 1970b). A collision without sliding takes place when the following condition is satisfied:

$$\left| u_{p1} - \frac{D_p}{2}\omega_{p1} \right| < \tfrac{7}{2}\mu_0(1+e)v_{p1}. \qquad [1]$$

For this condition, the subscript 1 refers to the particle velocity components before impact, e is the coefficient of restitution relating the normal velocity component after the collision to that before the collision, μ_0 is the static coefficient of friction and D_p is the particle diameter. Furthermore, u_p and v_p are the particle translational velocities parallel and normal to the wall, respectively, and ω_p is the angular velocity of the particle (figure 1). The particle translational and rotational velocities after rebound (subscript 2) are obtained from the impulse equations for the collision configuration shown in figure 1. For a *collision without sliding* one obtains:

$$\begin{aligned} v_{p2} &= -ev_{p1}, \\ u_{p2} &= \tfrac{1}{7}(5u_{p1} + D_p\omega_{p1}), \\ \omega_{p2} &= 2\frac{u_{p2}}{D_p}. \end{aligned} \qquad [2]$$

The velocity components after a *sliding collision* are calculated by

$$\begin{aligned} v_{p2} &= -ev_{p1}, \\ u_{p2} &= u_{p1} - \mu_d(1+e)v_{p1}\epsilon_0, \\ \omega_{p2} &= \omega_{p1} + 5\mu_d(1+e)\frac{v_{p1}}{D_p}\epsilon_0. \end{aligned} \qquad [3]$$

In these equations, μ_d is the dynamic friction coefficient and ϵ_0 indicates the direction of the relative velocity between the particle surface and the wall. It is given by

$$\epsilon_0 = \operatorname{sign}\left(u_{p1} - \frac{D_p}{2}\omega_{p1} \right). \qquad [4]$$

In the above equations the only empirical value is the coefficient of restitution, which strongly depends on the particle velocity, the collision angle and the material properties of the particle and the wall (Brauer 1980). The static and dynamic friction coefficients are generally known for certain material combinations although, depending on the properties of the wall surface, some scatter may be possible. Experimental studies (Tabakoff & Hamed 1977; Govan *et al.* 1989) have shown that the coefficient of restitution is subject to some scatter due to wall roughness and asphericities in the particle shape.

A numerical model for particle–wall collisions should, therefore, additionally consider the wall roughness and the resulting stochastic nature of the process. The influence of surface roughness on the collision process depends on the roughness structure which is a result of the manufacturing process and the range of particle size considered. The wall roughness may be characterized by a number of parameters, but the most important ones are the mean roughness depth (H_r) and the

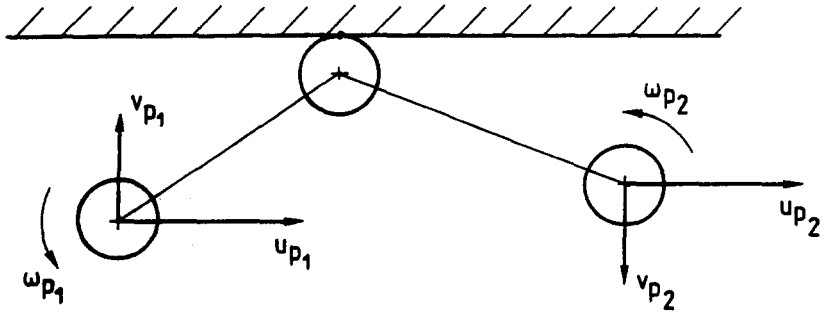

Figure 1. Configuration of a particle–wall collision.

mean cycle of roughness (L_r) (figure 2). When a small particle with a diameter less than the cycle of roughness ($D_p < L_r$) is considered, one may estimate the maximum change of the collision angle due to roughness by

$$\gamma_{max} = \arctan \frac{2H_r}{L_r}.$$

For particles larger than the cycle of roughness, the maximum roughness angle is reduced (figure 2). Assuming that the smallest roughness height is about $H_r/2$, the maximum roughness angle is given by

$$\gamma_{max} = \arctan \frac{H_r}{2L_r}.$$

For example, the roughness height for a machined metal plate lies typically in the range of 5–20 μm and the mean distance between the roughness peaks (i.e. roughness cycle) is about 10–20 times larger. This results in maximum roughness angles of $\gamma_{max} = \pm 11°$ to $\pm 5.7°$ for small particles and $\gamma_{max} = \pm 3°$ to $\pm 1.4°$ for large particles.

One of the first models which considers the influence of the wall roughness and the effect of particle shape on particle–wall bouncing was proposed by Matsumoto & Saito (1970a, b) and is based on a stochastic treatment of the collision process. In these studies the rough wall is represented by a sinusoidal shape, as shown in figure 3, whereby A_r is the amplitude of the waves and L_r is the cycle of the roughness. The phase of the roughness (α) was randomly sampled from

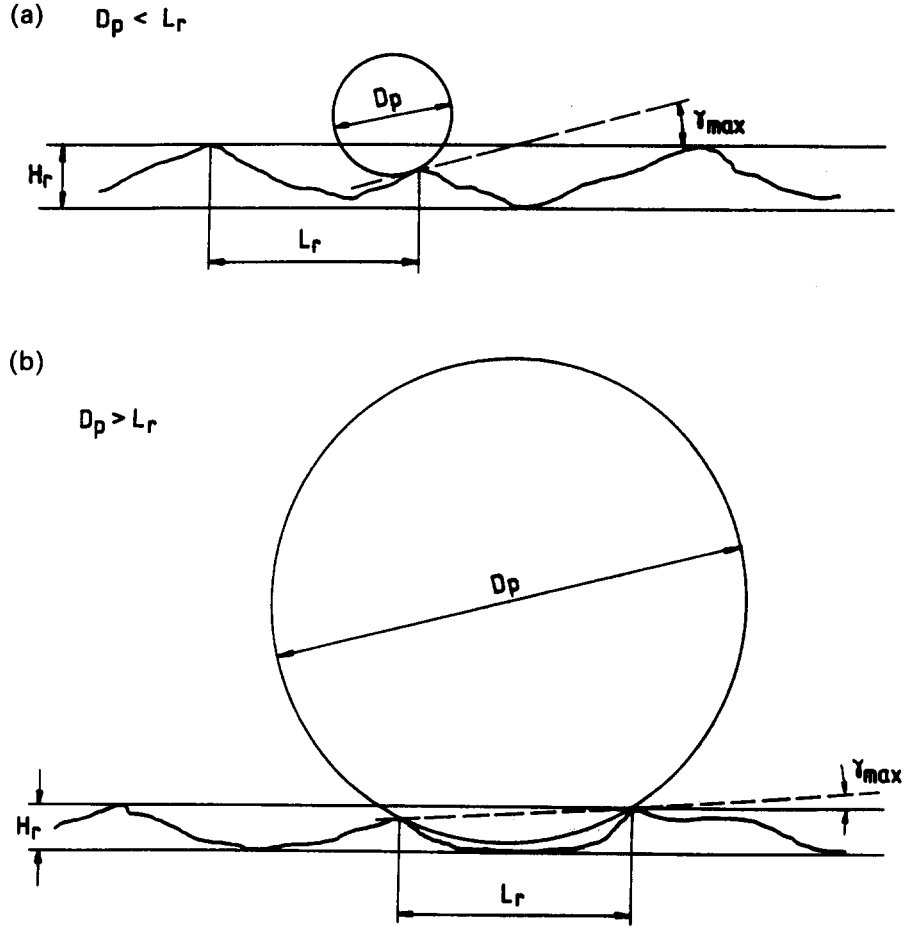

Figure 2. Effect of wall roughness on a particle–wall collision for (a) small particles and (b) large particles.

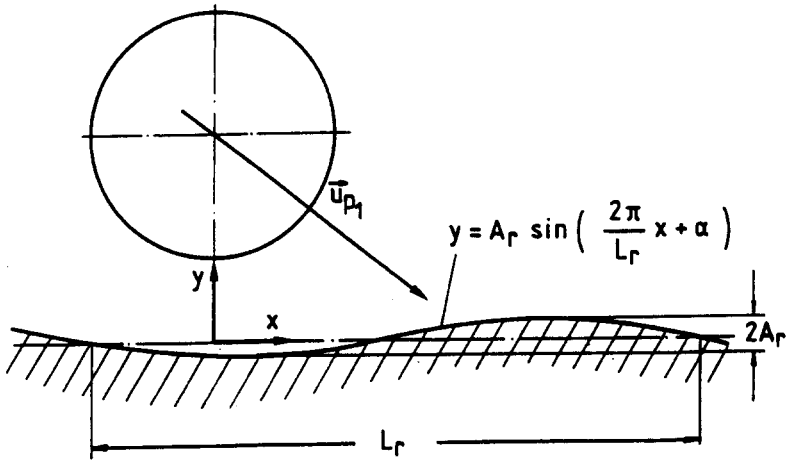

Figure 3. Irregular bouncing model of Matsumoto & Saito (1970b).

a uniformly distributed random number in the range $[0, 2\pi]$ in order to avoid a correlation between the particle collision point and the surface roughness.

For the calculation of the collision process, the impulse equations given above are applied after a transformation of the particle velocities to a coordinate system which is aligned with the statistically sampled local wall inclination. The comparison of numerical simulations with experimental results obtained in a horizontal two-phase channel flow by using 500 μm glass beads showed reasonable agreement for the particle velocity and concentration profiles at $L_r/D_p = 10$ and $A_r/D_p = 1/40$. The dynamic coefficient of friction was assumed to be 0.4 and the coefficient of restitution to be 0.97. The experiments of Matsumoto & Saito (1970b) were, however, conducted in a channel made of glass plates. The walls must therefore be regarded as smooth so that their model simulates the effect of slight non-sphericities in the particle shape rather than wall roughness, which also explains the choice of the model parameters.

Tsuji *et al.* (1985, 1987) considered the particle–wall collision for a pipe flow in a different fashion. Their "abnormal bouncing" model states that the plane wall is replaced by a virtual wall when the particle collision angle is below a certain value (figure 4). This method was introduced to eliminate particle settling, so as to conform with experimental observations.

The virtual wall increases the collision angle by a certain value γ, given by the following equations:

$$\gamma = \begin{cases} -\delta(\alpha_1 - \beta) & (\alpha_1 \leqslant \beta) \\ 0 & (\alpha_1 > \beta); \end{cases} \qquad [5]$$

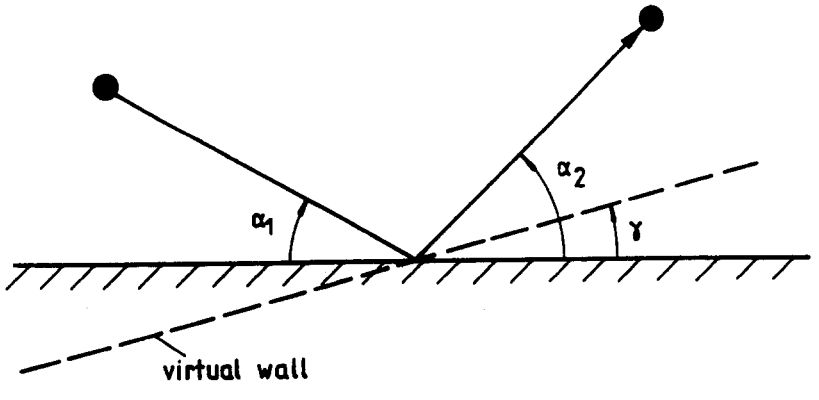

Figure 4. Abnormal bouncing model of Tsuji *et al.* (1985, 1987).

with

$$\delta = \frac{2.3}{\mathrm{Fr}} - \frac{91}{\mathrm{Fr}^2} + \frac{1231}{\mathrm{Fr}^3},$$

$$\beta = 7°,$$

$$\mathrm{Fr} = \frac{u}{\sqrt{g \cdot h}}, \qquad [6]$$

where Fr is the Froude number, h is the pipe diameter or channel height and g is the gravitational constant.

The foregoing empirical correlations were derived from two-phase pipe flow experiments. The randomness of the bouncing process is obtained by additionally introducing a randomly distributed yaw angle within certain limits. This angle determines the angle of reflection in the pipe cross-section.

Irregularities in the bouncing process for a horizontal channel flow (Tsuji *et al.* 1987) were introduced through a randomly distributed coefficient δ, according to

$$\delta = c \cdot R^k \cdot \delta_0, \qquad [7]$$

where $c = 5$, $k = 4$, δ_0 is obtained from [6] and R is a random number in the range [0, 1]. In the numerical simulations of Tsuji *et al.* (1987), the model described in [5]–[7] yielded reasonable agreement with experiments for the particle concentration and velocity at lower gas velocities ($\bar{u} = 7$ m/s). In the case of higher velocities ($\bar{u} = 15$ m/s), the particle concentration profile obtained by numerical simulation showed a large peak near the bottom of the channel, which was not observed in the experiments. However, a major drawback of the model introduced by Tsuji *et al.* is that it does not account for roughness effects in the collision process for collision angles larger than $\alpha_1 = 7°$. Hence, it does not reproduce the physical effects of such collisions, since the roughness effect is always present no matter what collision angle is considered.

The form of the model introduced by Sommerfeld (1990a) differs slightly, in that a random inclination of the wall with respect to the particle trajectory (figure 5) is assumed for all collision angles. The inclination of the virtual wall was assumed to be randomly distributed in the range $-4° < \gamma < 4°$ with equal probability (shaded area in figure 5). The results obtained using this model showed a considerable improvement in the prediction of the velocity fluctuations of the particle phase and a rather good agreement with the experimental results was achieved (Sommerfeld 1990a).

However, for further improvements additional numerical and experimental studies are necessary. Several models for particle–wall collisions are considered in this paper and the importance of the various parameters involved are studied by simulating the statistics of the wall bouncing process.

3. NUMERICAL SIMULATION OF PARTICLE–WALL COLLISIONS

One of the few sources of experimental information on the statistics of a particle–wall collision is the study of Grant & Tabakoff (1975). Hence, these results serve as a benchmark case for testing and validating the ability of the different models in simulating the correct statistics for an irregular particle–wall collision. The experiments have been performed using quartz sand with a mean

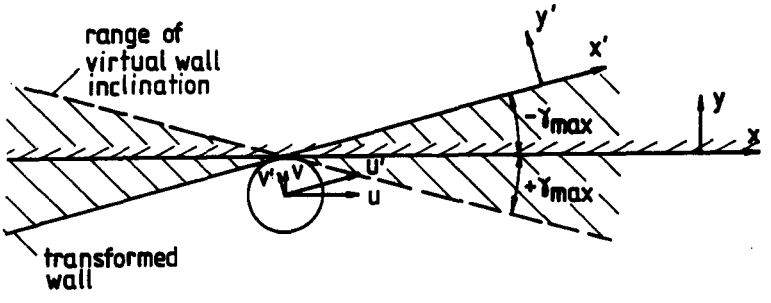

Figure 5. Irregular bouncing model of Sommerfeld (1990a).

diameter of $D_p = 200\,\mu$m. The particles were accelerated in a wind tunnel and then hit an aluminium target mounted in the wind tunnel far downstream of the particle injection point with a velocity of $u_p = 8.2$ m/s. Three models are compared in the numerical simulations:

Model 1. Model of Sommerfeld (1990a) with a uniformly distributed probability of the inclination γ of the virtual wall between $\pm\gamma_{max}$.
Model 2. Same as model 1, but with a Gaussian distribution of the wall roughness angle γ with a given standard deviation of $\Delta\gamma$ and a mean value of 0°.
Model 3. Model of Matsumoto & Saito (1970b) with $L_r/D_p = 3$ and $A_r/D_p = 1/20$ (for this case only one set of model parameters was considered).

All these models are based on the impulse equations for a particle–wall bouncing. The only input needed is the dependence of the coefficient of restitution on the collision angle and the static and dynamic friction coefficients. The static and dynamic friction coefficients were assumed to be $\mu_0 = 0.4$ and $\mu_d = 0.3$, respectively. The dependence of the normal coefficient of restitution on the collision angle was assumed to follow the relation obtained by Grant & Tabakoff (1975):

$$e = \frac{v_{p2}}{v_{p1}} = 0.993 - 1.76\alpha_1 + 1.56\alpha_1^2 - 0.49\alpha_1^3. \qquad [8]$$

In the calculations, 10,000 particles were simulated. These collided with the inclined target at a constant translational velocity and without rotation. For each collision, the virtual wall inclination was sampled according to the different models and the collision process was calculated based on the impulse equations, [1]–[4], in a coordinate system aligned with the virtual wall. The particle velocities after collision were finally obtained by re-transformation of the coordinate system and the probability density functions were sampled. In figure 6, the numerically simulated distributions of the normal coefficient of restitution obtained by the different models are compared with the experimental results of Grant & Tabakoff (1975) for two collision angles and different model parameters. The experimental results have been reproduced by assuming a Gaussian distribution function of the particle velocities after the collision with a mean value given by [8] and a standard deviation as given in Grant & Tabakoff (1975). The simulated results agree fairly well with the distributions obtained in the experiments. Please note that, in the numerical simulations, only the dependence of the mean normal restitution ratio on the collision angle was used as an input.

The comparison of the experiments with the simulations using the various collision models indicates that the best choice is model 2, where the randomness of the bouncing process was simulated by assuming a Gaussian distribution of the wall inclination with respect to the particle trajectory. This assumption results in a similar probability of restitution coefficients to that obtained by Grant & Tabakoff (1975) for the small collision angle when a standard deviation of $\Delta\gamma = 4°$ is used. For the larger collision angle of 45°, the simulated distribution is narrower than in the experiments, even when a standard deviation of the Gaussian distribution of $\Delta\gamma = 6°$ is used. This result indicates that the wall roughness models need to incorporate a dependence of the roughness effect on the collision angle.

Since in model 1 (Sommerfeld 1990a) a uniform distribution of the statistically distributed collision angle γ was assumed, the normal coefficient of restitution shows a constant probability in a certain range, depending on the value of γ_{max}. Even when a value of $\gamma_{max} = \pm 6°$ is used, the distribution of the normal coefficient of restitution shows no values above unity as observed in the experiment. The wall roughness model of Matsumoto & Saito (1970b) promotes the occurrence of large and small roughness angles, as a result of the assumption that the wall roughness is sinusoidal. This effect appears as a peak in the probability function for high and low coefficients of restitution. It follows that this model does not represent the statistical nature of the bouncing process of an irregular particle on a rough wall.

The probability distributions of the tangential veloctiy restitution ratio predicted with model 2 are narrower for both collision angles than those observed in the experiments (figure 7). It has to be noted that the double peak in the probability for a collision angle of 20° is due to the switching between sliding and non-sliding collision, [1]–[4]. Moreover, the simulated distribution function is not Gaussian in shape, as is the case in the results of Grant & Tabakoff (1975). The increase in

the standard deviation of the roughness distribution in model 2 only results in a slightly broader distribution of the tangential restitution ratio. This result suggests that more sophisticated correlations for the friction coefficients are required in the model which include the influence of the collision angle.

The friction coefficient between the particle and the wall depends mainly on the combination of materials. It determines the domain of the collision angles in which sliding or non-sliding collisions occur (see [1]). The boundaries between the two collision types are indicated in figure 8 for different coefficients of restitution. With decreasing wall friction, the minimum collision angle for which sliding collisions occur increases and a lower coefficient of restitution additionally extends the domain of sliding collisions. This implies that in pneumatic conveying, where collision angles are usually small, sliding collisions will occur the most frequently.

It has been proposed in several studies (e.g. Matsumoto & Saito 1970a, b) that particle rotation has a significant influence on the particle–wall bouncing. In order to investigate the effect of particle

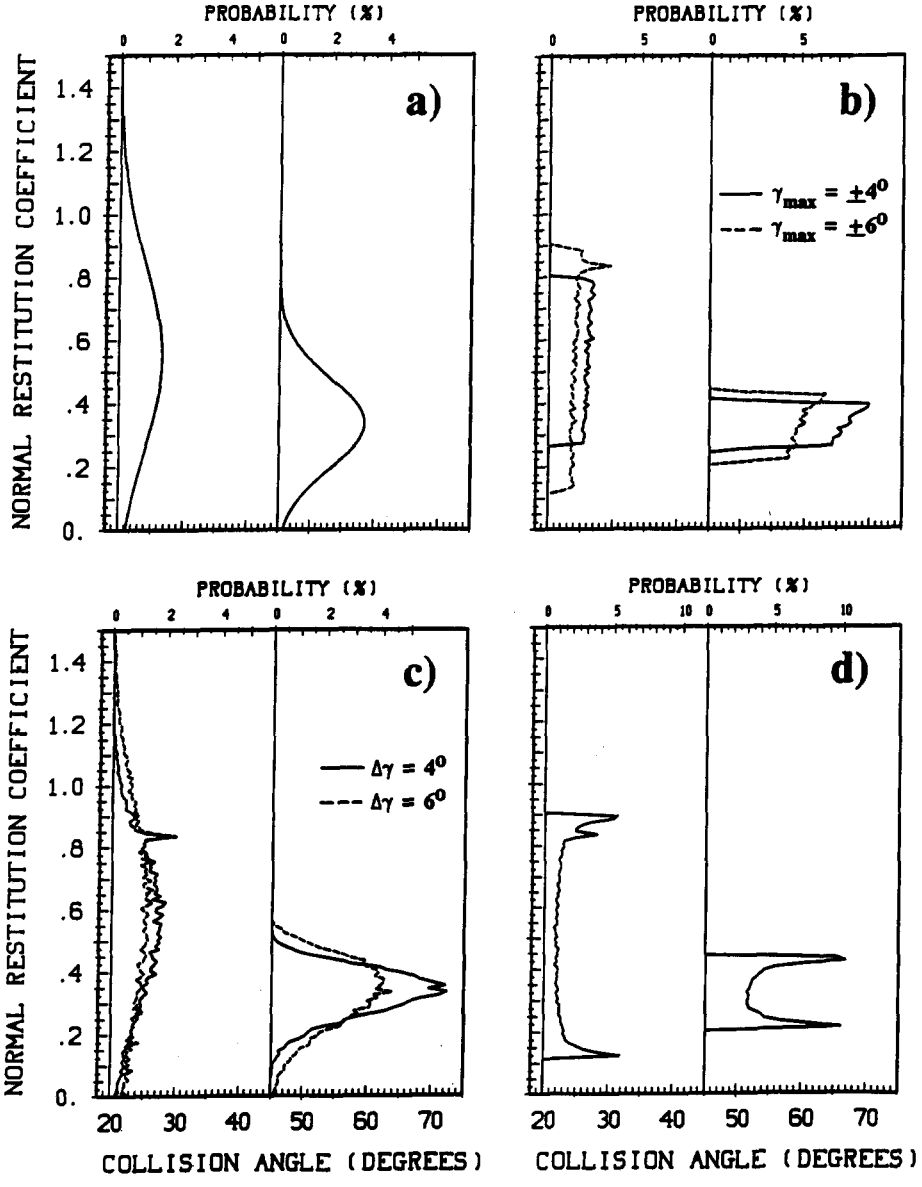

Figure 6. Normal coefficient of restitution (note that the probability scales are not identical for the different models): (a) experiments of Grant & Tabakoff (1975); (b) numerical simulation model 1; (c) numerical simulation model 2; (d) numerical simulation model 3.

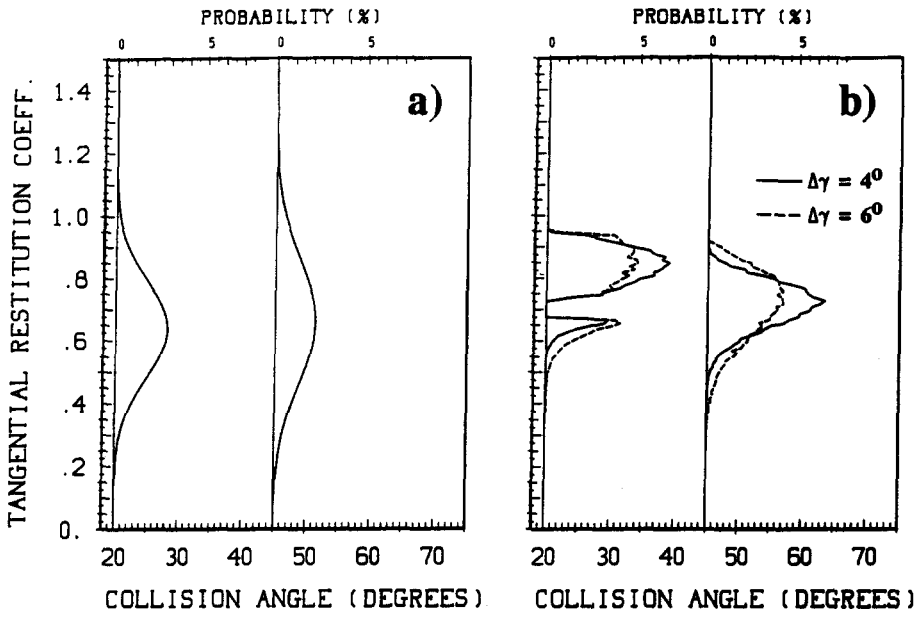

Figure 7. Tangential velocity restitution ratio: (a) experiments of Grant & Tabakoff (1975); (b) numerical simulation model 2.

rotation on the collision process, the boundaries between sliding and non-sliding collision are calculated using [1] for different initial particle velocities. The results are plotted as a function of the collision angle in figure 9. On the right-hand side of the different curves a non-sliding collision will occur, while on the left-hand side a sliding collision will be observed. The effect of particle rotation on the type of wall collision only becomes important for particles with high rotational and low translational velocities. The influence of the rotation is to extend the domain for non-sliding collisions towards smaller collision angles for positive particle rotations and towards larger collision angles for negative rotations, respectively. As the wall friction increases, the domain over which sliding collisions occur becomes smaller, i.e. a non-sliding collision is already observed at smaller collision angles.

Based on [2] and [3], the translational velocities after the rebound of the particle are only influenced by their rotation for the case of a collision without sliding. In this situation, the particle velocity parallel to the wall may increase or decrease depending on the direction of rotation. In the case of irregular bouncing, numerical simulations using the conditions given at the beginning of this section show that the distribution of the coefficients of restitution is not influenced

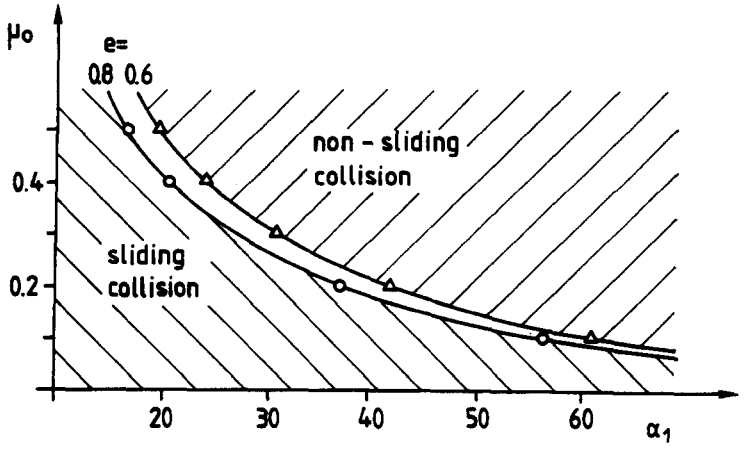

Figure 8. Domains of collision type depending on the friction and coefficient of restitution.

considerably by the particle rotation when, for example, a Gaussian distribution for the particle rotation with a mean value of 1500 rps is assumed. A further, detailed evaluation of the influence of particle rotation on the wall-collision process for small angles of incidence below about 20° is, however, still necessary for a refinement of the collision models.

4. NUMERICAL SIMULATION OF A CHANNEL FLOW

Previous numerical simulations of the particle dispersion in a plane turbulent channel flow (Milojevic *et al.* 1986; Sommerfeld & Zeisel 1988; Sommerfeld 1990b) showed a considerable decay of the particles' velocity fluctuation along the flow direction, especially for the larger particles ($\overline{D_p} = 108\ \mu$m). Since the motion of these rather large particles is strongly influenced by particle–wall collisions, a more realistic model for the particle–wall bouncing ought to have considerable influence on the properties of the particle field (i.e. axial mean velocity, velocity fluctuation and particle concentration). This fact can be seen in a recent publication (Sommerfeld 1990a), in which the numerical simulation incorporating the irregular bouncing model 1 (see the previous section) was compared with the results obtained for an ideal and elastic particle–wall collision. The comparison of the numerical simulations with the experiments (Milojevic *et al.* 1986) showed that the numerical results for the particle mean velocity and the mass flux were not affected substantially by the irregular particle bouncing and that these results agreed well with the experiments for all the cases considered. The particle velocity fluctuation, however, was considerably higher and a better agreement with the experiments was obtained for the simulations

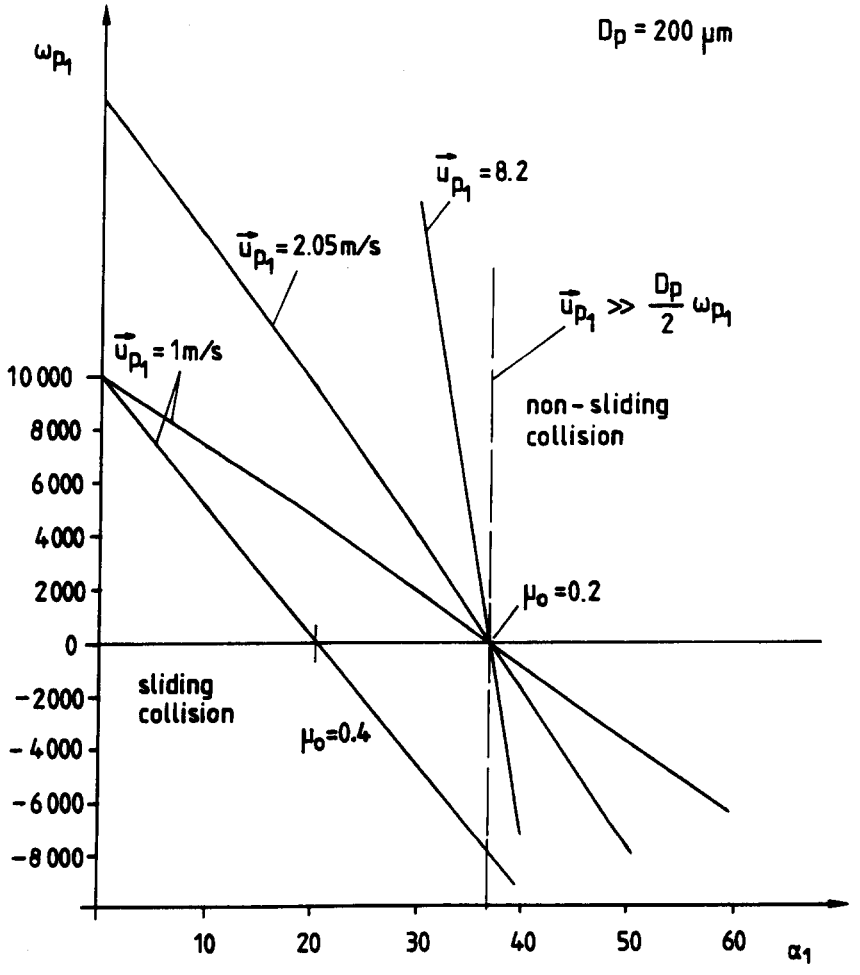

Figure 9. Influence of particle rotation on the type of collision.

incorporating the irregular bouncing model, as compared with those obtained with the ideal particle–wall collision model. In the present calculations, the results obtained using a Gaussian probability distribution function to model the roughness angle are compared to previous results (Sommerfeld 1990a).

For completeness, the basic equations for the particle phase and the numerical procedure are reviewed briefly. The numerical calculations for the prediction of the fluid flow are based on the time-averaged Navier–Stokes equations and are performed by the CAST code (Peric *et al.* 1988), which incorporates the well known k–ϵ, two-equation turbulence model. This code uses a finite volume scheme to discretize the basic equations.

The particle phase is treated by the Lagrangian approach, wherein after injection at the inlet all the particles are traced simultaneously through the flow field (Sommerfeld 1990b). The influence of the particle phase on the fluid properties is neglected since only a very dilute two-phase system is considered. In addition to the drag and gravity force, the slip-shear lift force introduced by Saffman (1965) and the slip-rotation lift force derived by Rubinow & Keller (1961) are introduced in the particles' equation of motion. The added mass effect and the Basset history force can be neglected for gas–solid systems, since the density ratio ρ_p/ρ is very large. This results in the following set of equations to determine the new locations and velocities of the particles:

$$\frac{dx_p}{dt} = u_p, \quad \frac{dy_p}{dt} = v_p, \tag{9}$$

$$\frac{du_p}{dt} = \frac{3\rho c_D (u - u_p)|\mathbf{u} - \mathbf{u}_p|}{4\rho_p D_p} - g - \frac{3}{4}\frac{\rho}{\rho_p}\left[\frac{1}{2}\left(\frac{\partial v}{\partial x} - \frac{\partial u}{\partial y}\right) - \omega_p\right](v - v_p) \tag{10}$$

and

$$\frac{dv_p}{dt} = \frac{3\rho c_D (v - v_p)|\mathbf{u} - \mathbf{u}_p|}{4\rho_p D_p} + \frac{9.69(\rho\mu)^{0.5}}{\pi\rho_p D_p}\left|\frac{du}{dy}\right|^{0.5}(u - u_p) + \frac{3}{4}\frac{\rho}{\rho_p}\left[\frac{1}{2}\left(\frac{\partial v}{\partial x} - \frac{\partial u}{\partial y}\right) - \omega_p\right](u - u_p). \tag{11}$$

The following correlations for the drag coefficient (c_D) as a function of the particle Reynolds number (Re_p) are used:

$$c_D = \begin{cases} \dfrac{24.0}{Re_p}(1.0 + \frac{1}{6}Re_p^{0.66}) & Re_p < 1000 \\ 0.44 & Re_p > 1000; \end{cases} \tag{12}$$

with

$$Re_p = \frac{\rho D_p |\mathbf{u} - \mathbf{u}_p|}{\mu},$$

$$|\mathbf{u} - \mathbf{u}_p| = \sqrt{(u - u_p)^2 + (v - v_p)^2}. \tag{13}$$

The change in the particle's angular momentum due to its interaction with the surrounding fluid is given by (Rubinow & Keller 1961):

$$\frac{d\omega_p}{dt} = \frac{60\mu}{D_p^2 \rho_p}\left[\frac{1}{2}\left(\frac{\partial v}{\partial x} - \frac{\partial u}{\partial y}\right) - \omega_p\right]. \tag{14}$$

The interaction of the particles with flow turbulence is modelled by a stochastic approach (e.g. Gosman & Ioannides 1983; Milojevic 1990; Sommerfeld 1990b). The instantaneous fluid velocity along the particle trajectory used in [9]–[14] is sampled from a Gaussian velocity distribution with the RMS value of

$$\sqrt{\overline{u'^2}} = \sqrt{\frac{2}{3}k}. \tag{15}$$

This instantaneous fluid velocity is assumed to influence the particle motion during a given time period, the interaction time, before a new fluctuation component is sampled from the Gaussian distribution function. In the present model, the successively sampled fluid velocity fluctuations are

assumed to be uncorrelated. The interaction time of a particle with the individual, simulated turbulent eddies is governed by two criteria:

- The random lifetimes of the turbulent eddies are determined by a Poisson process where a random variable RN is sampled from a uniform probability distribution between 0 and 1. When this random variable becomes smaller as the ratio $\Delta t/T_L$, where Δt is the time step size and T_L is the Lagrangian integral time scale of the turbulence, a new fluctuation is generated. The Lagrangian integral time scale is calculated from the turbulent kinetic energy k and the dissipation rate ϵ in the following way:

$$T_L = C_T \frac{k}{\epsilon}, \qquad [16]$$

  where c_T was determined to be 0.3 by calibrating the calculations with the experimental results of Snyder & Lumley (1971). This process results in an exponential form of the particle velocity autocorrelation (Ormancey & Martinon 1984).
- The crossing trajectory effect is accounted for by integrating the distance which the particle travels through the eddy and comparing it with the characteristic length scale of the eddy $L_E = T_L u'$. As soon as the particle leaves the eddy, a new fluctuation component is sampled.

For the particle–wall collision process, three models are considered where the model parameters have been selected based on the results obtained in section 3:

Case A. Particle–wall collision based on [1]–[4] (elastic wall collision).
Case B. Same as case A but with the irregular particle bouncing model where a uniform distribution of the inclination of the virtual wall between $-4° < \gamma < 4°$ is assumed (Sommerfeld 1990a).
Case C. Same as case A but with a Gaussian distribution of the virtual wall inclination with a standard deviation of $\Delta\gamma = 4°$ and a mean value of 0°.

It should be noted that in particle-laden channel or pipe flows the particle collision angles with the walls are usually very small. Therefore, it may happen that when a negative roughness angle is sampled in the irregular bouncing models, the resulting collision angle becomes negative (i.e. the particle would be outside the wall). Under such circumstances it is assumed that the particle first hits a roughness structure with positive inclination. That is, the sign of the roughness angle is changed from negative to positive. For the static and dynamic friction coefficients, the values of 0.4 and 0.3 were used and the normal coefficient of restitution was assumed to decrease linearly from 1.0 to 0.9 for collision angles between 0° and 30° (Brauer 1980). For larger collision angles, the coefficient of restitution was assumed to have a constant value of 0.9.

The flow configuration is the same as in Sommerfeld (1990a). A plane gas particle jet mixes with two co-flowing plane jets within a vertical channel. The walls of the channel were made of milled aluminium alloy plates. The roughness has not been analysed, but it can be assumed that the roughness height is about 10–20 μm. The configuration of the channel together with the velocity profiles of the gas and particles at the inlet are shown in figure 10. Two flow conditions with different particles are considered. The particles were spherical glass beads ($\rho_p = 2.5$ g/cm^3) with a mean number diameter of 45 and 108 μm, respectively. The size distributions of both kinds of particles are given in figure 11 and the numerical simulations are performed by considering these distribution functions (Sommerfeld 1990b). The particle mass loading in the central channel was 0.02 for the flow condition with the small particles and 0.17 for the large particles. Therefore, the influence of the particles on the gas phase may be neglected.

The motion of the small particles is not supposed to be strongly influenced by particle–wall collisions, while the flow condition for the large particles is most likely to fall into the category "wall-collision-dominated" two-phase flow. The behaviour of the different sized particles in the channel flow is demonstrated by numerical simulations of the particle trajectories starting at the

edge of the central channel (figure 12). Since the flow is symmetric with respect to the centreline only one half of the channel is shown in figure 12.

In the case of the small particles (i.e. 45 μm) no considerable difference is observed in the particle trajectories for the calculations with and without the irregular bouncing model, since the wall-collision probability is rather low [figure 12(a)]. Although the particles disperse in different directions from the injection point due to their initial velocitiy fluctuations, they are quickly entrained by the flow. The "wavy" form of the particle trajectories is a result of the interaction with flow turbulence.

The large glass beads emanate from the injection point in a similar fashion. However, their trajectories are rather straight compared with those for the small beads, due to their larger inertia. This implies that a number of particles collide with the channel wall, bounce off the wall and eventually collide with the opposite wall [figure 12(b)]. The distance which is necessary for a particle to acquire a considerable velocity change due to the interaction with the surrounding fluid may be obtained by multiplying the Stokesian response time by the average particle velocity at the inlet. For this case, the distance is about 0.79 m. The characteristic distance from the inlet where the

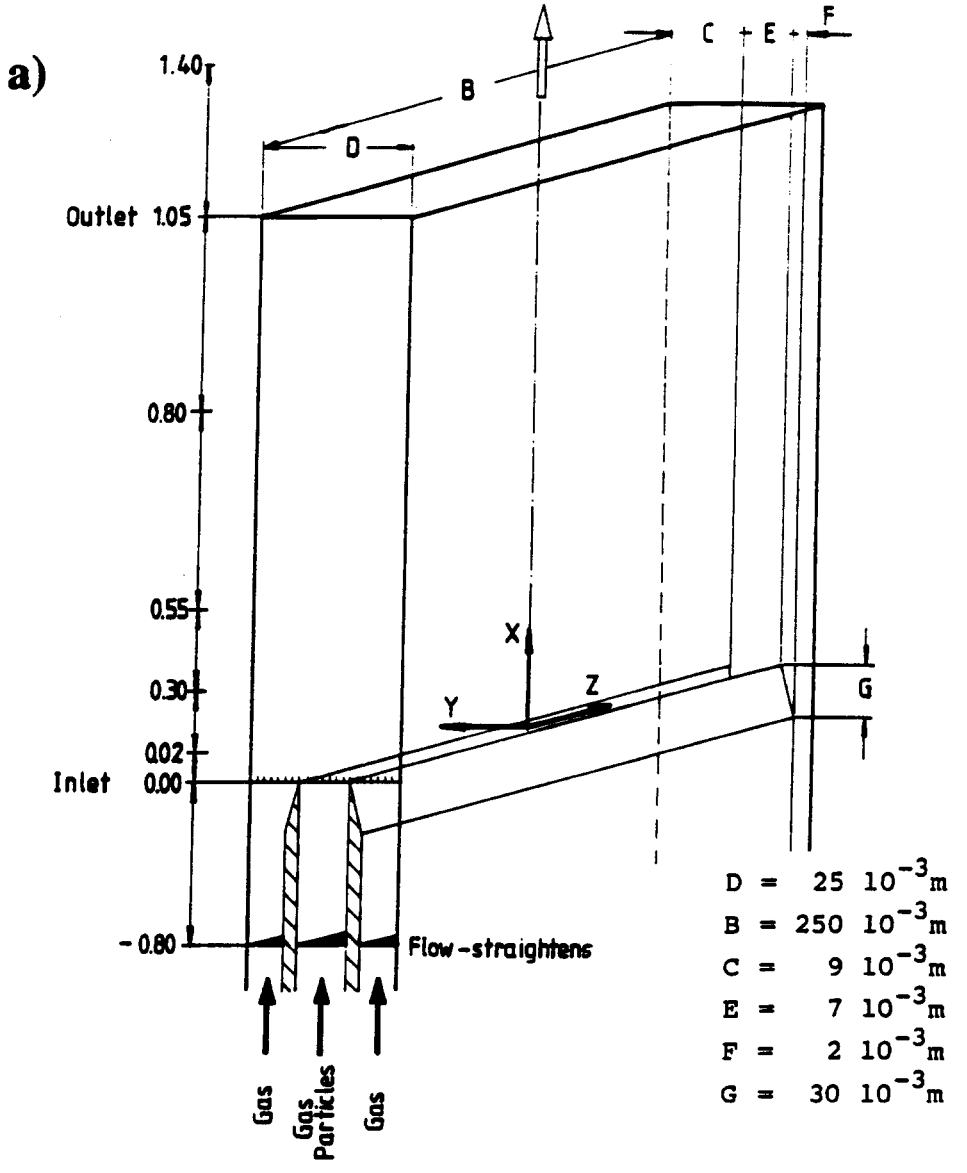

Figure 10—*caption opposite.*

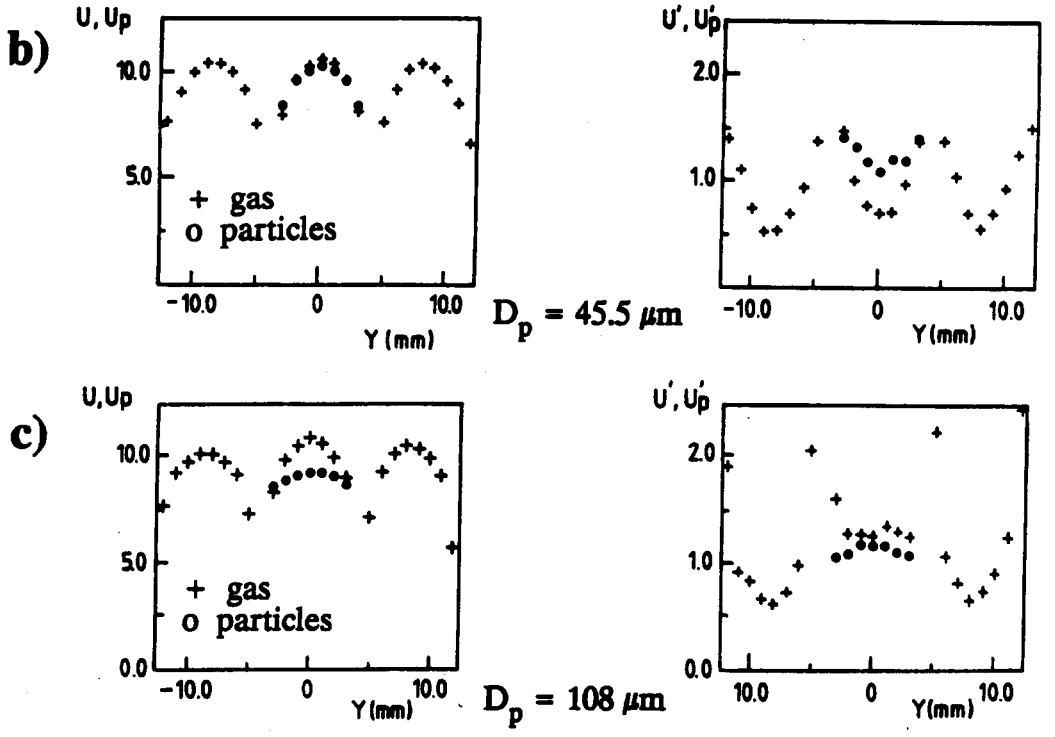

Figure 10. Channel flow (Milojevic *et al.* 1986): (a) configuration of the test section; (b) axial mean velocities and RMS values at the inlet for $\overline{D_p} = 45\,\mu$m; (c) axial mean velocities and RMS values at the inlet for $\overline{D_p} = 108\,\mu$m.

particles reach the wall may be obtained from the transverse velocity fluctuation and the mean axial particle velocity at the inlet ($v_p' = 0.35$ m/s and $\overline{u_p} = 9$ m/s):

$$L = \frac{D\overline{u_p}}{v_p'} = 0.64.$$

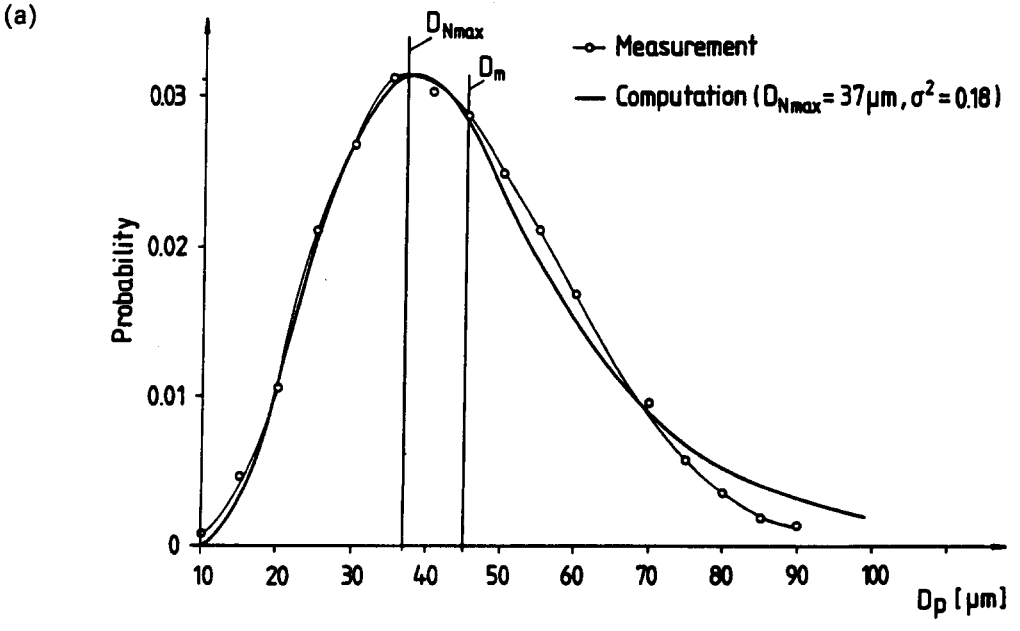

Figure 11—*caption overleaf.*

(b)

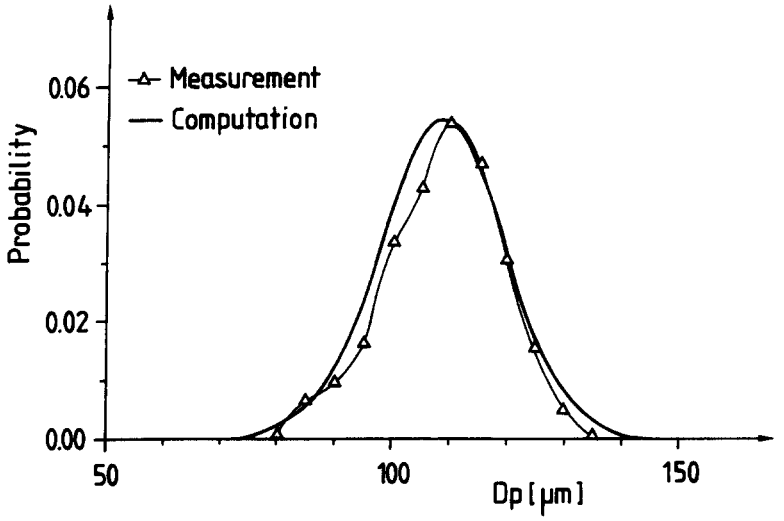

Figure 11. Size distribution of the glass beads: (a) $\overline{D_p} = 45\ \mu m$; (b) $\overline{D_p} = 108\ \mu m$.

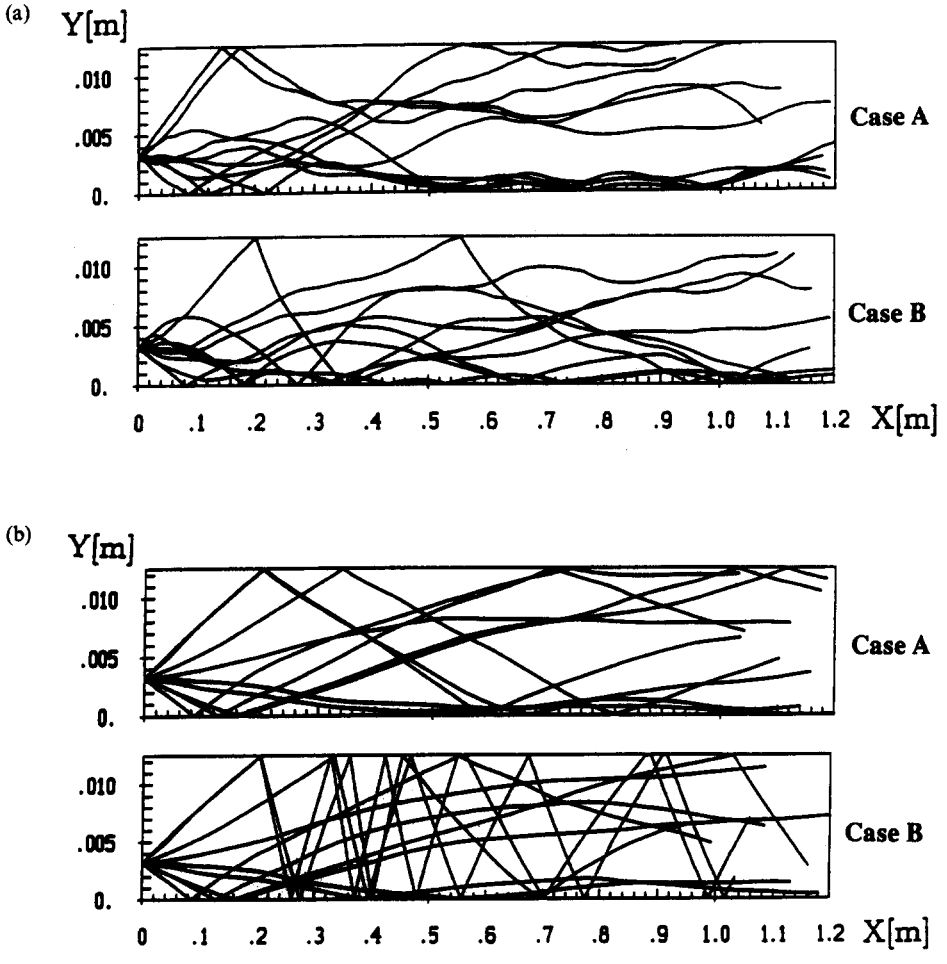

Figure 12. Particle trajectories for the wall-collision models of cases A and B (due to the symmetry of the flow field only one half is shown): (a) $\overline{D_p} = 45\ \mu m$; (b) $\overline{D_p} = 108\ \mu m$.

A comparison of the characteristic length scales indicates that the motion of the 108 μm particles is dominated by wall collisions. The interaction between the particles and the fluid turbulence is less important than that with the mean flow. The numerically simulated particle trajectories obtained with the wall-collision model in case A show that the particle trajectories are already fairly well aligned with the flow direction at about 1 m from the inlet and, as a consequence, the particle velocity fluctuations have decayed [figure 12(b)]. By introducing the irregular bouncing model (case B), the particles' zig-zag motion is enhanced and thus the particles continue to bounce between the walls throughout the test section.

The effect of wall roughness on the particle motion in the channel flow may also be made evident by comparing the computed particle collision angles α_1 samples between $x = 1000$ and 1100 mm (figure 13). The numerical simulations without roughness (case A) show that the collision angles for large particles are distributed between 0.5° and 2° with a mean value of $\overline{\alpha_1} = 1.1°$, whereas those for the small particles are within the range 0.5°–3° with a mean value of $\overline{\alpha_1} = 1.5°$. The slightly larger collision angles for the small particles reflect the effect of the flow turbulence on the particle motion. The numerical simulations using the irregular bouncing model (case C) yield much larger collision angles for both particle sizes. For the 108 μm particles, collision angles of up to 50° and a mean value of $\overline{\alpha_1} = 13°$ are predicted. Since small particles follow the gas flow more easily, their motion is less affected by the wall roughness. Thus, collision angles up to 20° are sampled between $x = 1000$ and 1100 mm and the mean collision angle is only 4.2°, which is slightly larger compared with the result without irregular bouncing.

The numerical simulations using the wall-collision models of cases A–C are compared with the experimental results in figure 14 for the small particles and in figure 15 for the large particles. The axial particle mean velocity and fluctuation velocities, as well as the particle mass flux, are shown at four different locations downstream of the inlet. As demonstrated previously (Sommerfeld 1990b), the predicted and experimental values for the gas phase correlate well except for slight differences in the gas-phase velocity fluctuations near the wall, which may be caused by the anisotropic nature of the near-wall turbulence.

Although the motion of the small particles ($\overline{D_p} = 45$ μm) is not considerably affected by the wall collisions, some important differences are observed between the calculations with the irregular bouncing model (case C) and the elastic wall-collision model (case A). The results for case B are similar to those obtained with case C and are therefore omitted. The fluctuation of the axial particle velocity increases slightly in the developed flow region (i.e. $x = 550$ and 1050 mm) for the calculation with the wall-roughness model. A slightly better agreement with the experiments is achieved near the centre line compared with the calculations using the elastic wall-collision model (figure 14). Outside this core region, both models slightly underpredict the axial particle velocity fluctuation, while at $x = 100$ mm, the particles' velocity fluctuation is predicted to be higher than observed experimentally. This, however, may be related to the overpredictions of the gas-phase turbulent kinetic energy in the initial mixing region of the flow (Sommerfeld 1990b). Furthermore, the increase in the particle mass flux near the wall at $x = 550$ and 1050 mm is avoided by applying the irregular bouncing model and the particle mass flux near the centreline increases, which results in better agreement with the experimental values. The axial particle mean velocity is not influenced strongly by the choice of the wall-collision model (figure 14). The numerical simulations slightly underpredict the axial velocity component in the region far downstream of the inlet ($x = 550$ and 1050 mm), which may be caused by the three-dimensional effects in the measurements.

The effect of the wall-collision models on the predicted particle phase properties is more pronounced for the large particles ($\overline{D_p} = 108$ μm). Considering the predicted particle properties in the development region ($x = 100$ mm) reasonable agreement with the measurements is achieved (figure 15). Only the particles' velocity fluctuation near the centreline is slightly underpredicted and the axial mean particle velocity profile is predicted to be flatter, as in the experiment. These results are independent of the collision model since the particles had not yet collided with the wall at this location (see figure 12).

Far downstream of the inlet ($x = 550$ and 1050 mm), remarkable differences in the particle phase properties result from the different collision models, except for the particle mass flux which is almost identical for all models. The agreement with the measured particle mass flux is quite good, except for the downstream location $x = 550$ mm where the predicted particle mass flux profile is

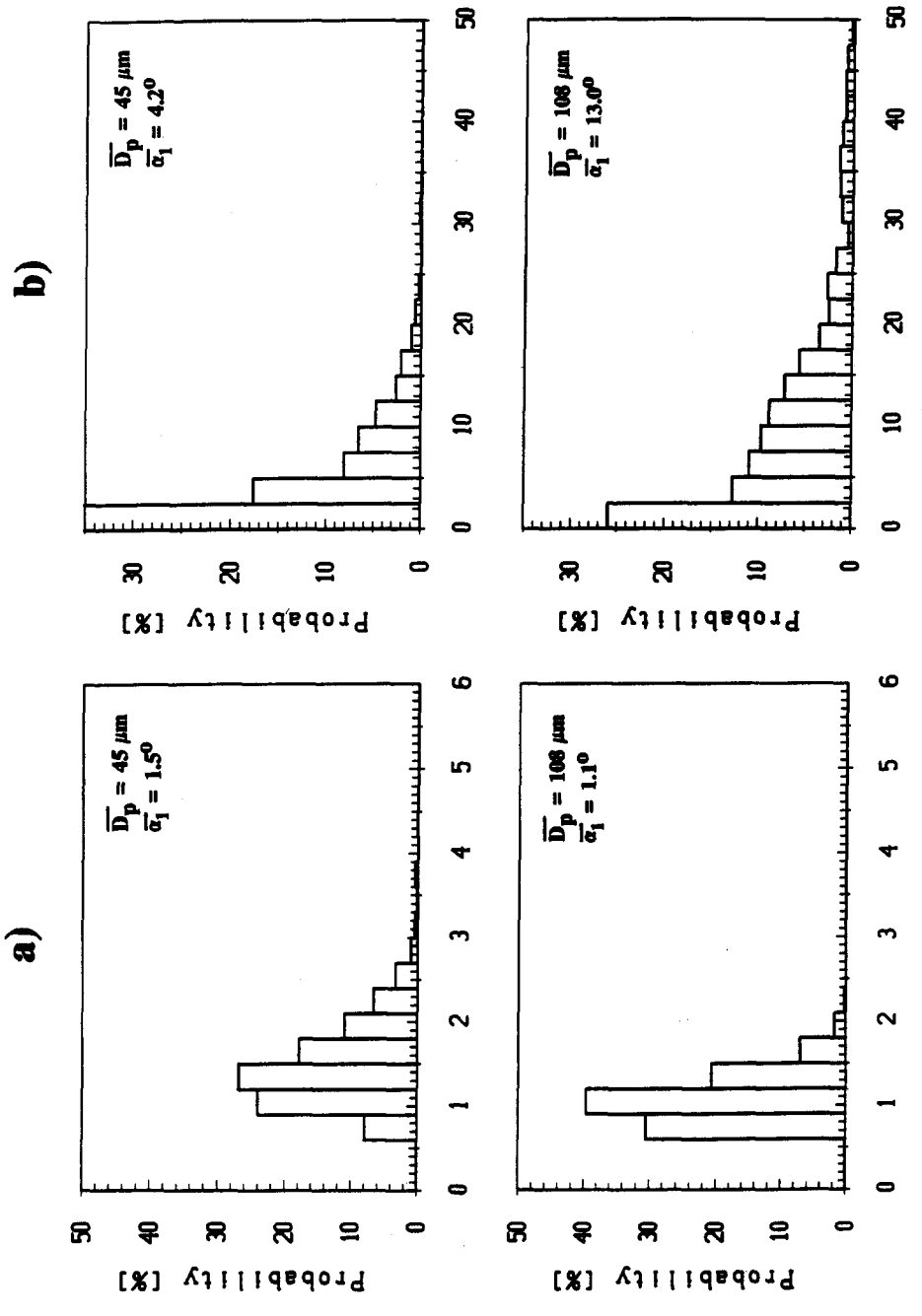

Figure 13. Numerically simulated probability distributions of the particle collision angle α_1 between $x = 1000$ and 1100 mm for small ($\overline{D_p} = 45\ \mu m$) and large particles ($\overline{D_p} = 108\ \mu m$): (a) collision model case A; (b) collision model case C.

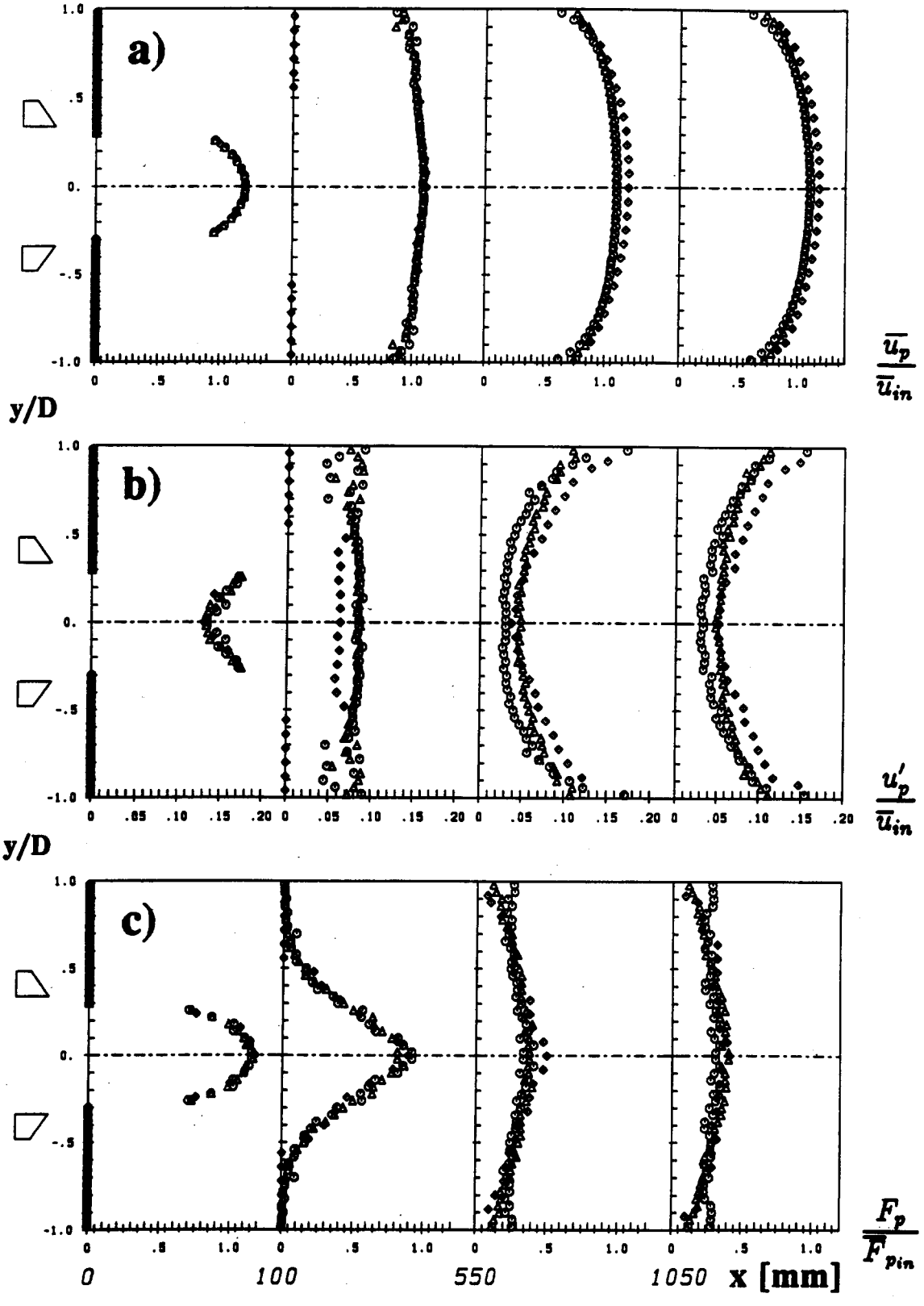

Figure 14. Comparison of the numerical simulations with the experiment for small particles, $\overline{D_p} = 45\ \mu$m (○, case A; △, case C; ◇, experiment): (a) normalized axial mean velocity of the particles; (b) normalized axial velocity fluctuation of the particles; (c) normalized particle mass flux.

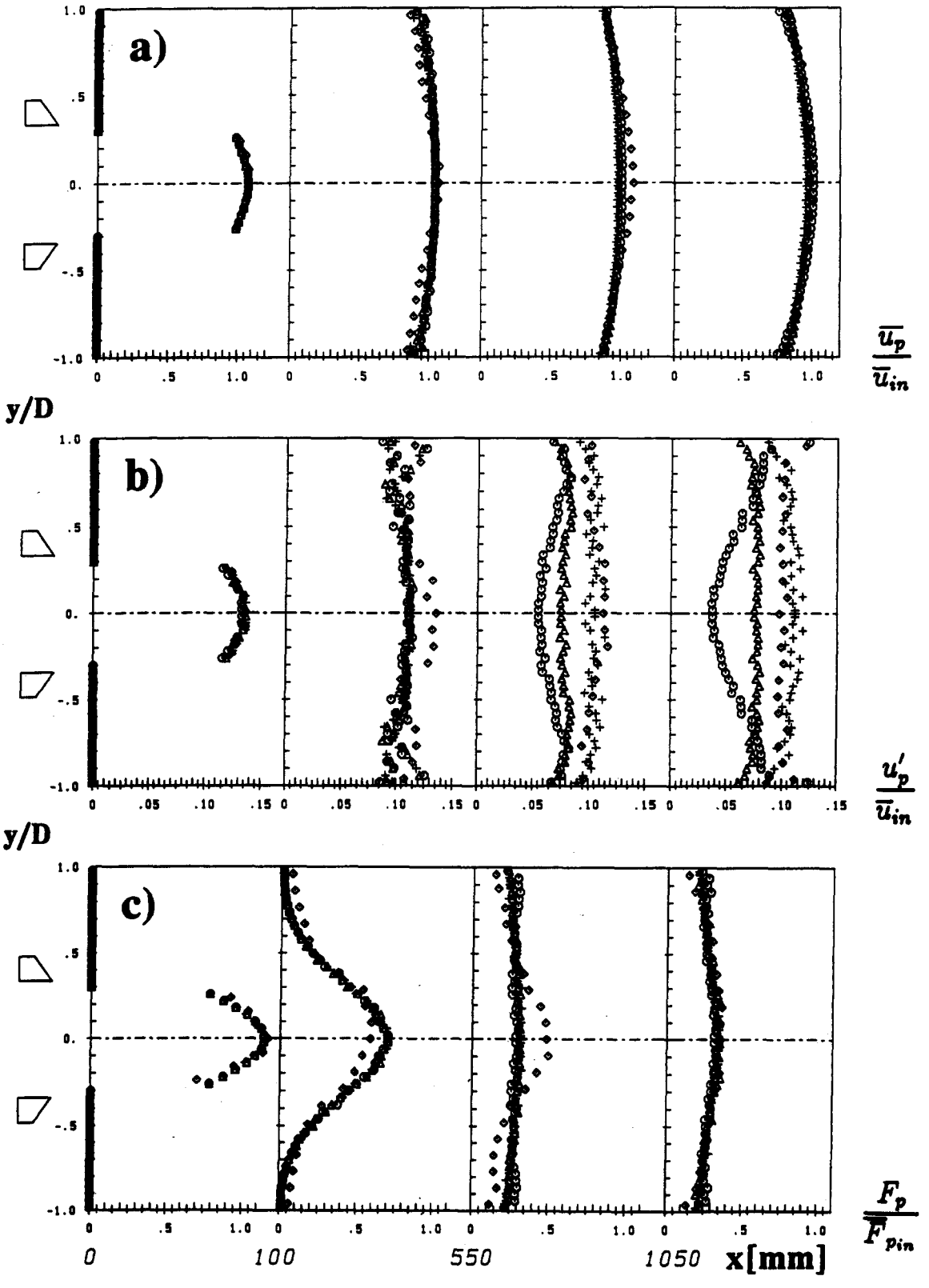

Figure 15. Comparison of the numerical simulations with the experiment for large particles, $\overline{D_p} = 108\ \mu m$ (○, case A; △, case B; +, case C; ◇, experiment): (a) normalized axial mean velocity of the particles; (b) normalized axial velocity fluctuation of the particles; (c) normalized particle mass flux.

considerably flatter than observed in the experiment. The profile of the axial mean particle velocity is flattened when the irregular bouncing model is employed since, in many cases, the irregular bouncing increases the transverse velocity component and reduces the axial component (see figure 12). This results in a slightly better agreement with the measured velocities. Major differences for the three collision models are observed in the particles' velocity fluctuation. Under the assumption of an ideal, elastic wall collision (case A) a considerable decay of the particle velocity fluctuation is predicted, which could not be observed in the experiments where the velocity fluctuations remain almost constant from $x = 100$ mm up to $x = 1050$ mm and have nearly constant values across the channel. This unrealistic decay does not occur when using the irregular bouncing model and a constant distribution of the particle velocity fluctuations across the channel is predicted. The wall-collision model with the Gaussian distribution of the random wall inclination gives excellent agreement with the measurements far downstream of the inlet ($x = 550$ and 1050 mm). The wall-roughness model with a constant probability of the roughness angle (case B) results in lower values for the particles' velocity fluctuations.

5. CONCLUSION

The results obtained with different particle–wall collision models based on the impulse equations and a statistical treatment of the wall surface roughness as well as irregularities in the particle shape show that such models adequately simulate the statistics of a collision process. The best agreement with particle–wall bouncing experiments was obtained for a model which assumes a Gaussian distribution for the roughness angle.

In the numerical simulation of confined turbulent particulate two-phase flow, the particle–wall collision modelling proved to be very important for predicting the particle dispersion characteristics in the case of larger particles, where the particles' relaxation length is larger than the characteristic dimension of the confinement. On the whole, the particle velocity fluctuations were increased considerably when irregular bouncing models were incorporated in the calculations. These results agree well with experimental ones. Furthermore, for the small particle flow condition, some important alterations of the particle phase properties have been observed when using the wall-collision models which incorporate the effect of the wall roughness. However, when comparing the simulations with those using the ideal wall-collision models the modifications of the particle phase properties for the small particles are less pronounced than for the large particles.

For a further refinement of the particle–wall collision models, detailed experiments which take into account the combination of particle and wall material and the roughness of the wall are necessary. In particular, for collision angles $< 10°$, which are typical for channel and pipe flows, no experimental data are available. More refined models should, furthermore, automatically simulate the effect of the wall roughness for different particle sizes since, in general, the particles are not monodisperse.

REFERENCES

BERLEMONT, A., DESJONQUERES, P. & GOUESBET, G. 1990 Particle Lagrangian simulation in turbulent flows. *Int. J. Multiphase Flow* **16,** 19–34.

BRAUER, H. 1980 Report on investigations on particle movement in straight horizontal tubes, particle–wall collision and erosion of tubes and tube bends. *J. Powder Bulk Solids Technol.* **4,** 3–12.

DURST, F. & RASZILLIER, H. 1989 Analysis of particle–wall interaction. *Chem. Engng Sci.* **44,** 2871–2879.

ELGHOBASHI, S. E. & ABOU-ARAB, T. W. 1983 A two-equation turbulence model for two-phase flows. *Phys. Fluids* **26,** 931–938.

GOSMAN, A. D. & IOANNIDES, E. 1983 Aspects of computer simulation of liquid-fueled combustors. *J. Energy* **7,** 482–490.

GOVAN, A. H., HEWITT, G. F. & TERRY, J. W. 1989 Measurements of particle motion in a turbulent pipe flow using an axial-viewing technique. In *Proc. Int. Conf. on Mechanics of Two-phase Flows,* pp. 103–109.

GRANT, G. & TABAKOFF, W. 1975 Erosion prediction in turbomachinery resulting from environmental solid particles. *J. Aircraft* **12,** 471–478.

MATSUMOTO, S. & SAITO, S. 1970a On the mechanism of suspension of particles in horizontal pneumatic conveying: Monte Carlo simulation based on the irregular bouncing model. *J. Chem. Engng Japan* **3,** 83–92.

MATSUMOTO, S. & SAITO, S. 1970b Monte Carlo simulation of horizontal pneumatic conveying based on the rough wall model. *J. Chem. Engng Japan* **3,** 223–230.

MILOJEVIC, D. 1990 Lagrangian stochastic-deterministic (LSD) prediction of particle dispersion in turbulence. *Particles Particle Syst. Charact.* **7,** 181–190.

MILOJEVIC, D., BÖRNER, TH. & DURST, F. 1986 Prediction of turbulent gas–particle flows measured in a plane confined jet. In *PARTEC; Reprints 1st Wld Congr. on Particle Technology*, Part IV, pp. 485–505.

OESTERLE, B. 1989 Internal kinetic transfers in the dispersed phase of a low concentration suspension flow. *Int. J. Multiphase Flow* **15,** 155–171.

ORMANCEY, A. & MARTINON, J. 1984 Prediction of particle dispersion in turbulent flows. *PhysicoChem. Hydrodynam.* **5,** 229–244.

PERIC, M., KESSLER, R. & SCHEURER, G. 1988 Comparison of finite-volume numerical methods with staggered and colocated grids. *Computers Fluids* **16,** 389–403.

RUBINOW, S. I. & KELLER, J. B. 1961 The transverse force on spinning sphere moving in a viscous fluid. *J. Fluid Mech.* **11,** 447–459.

SAFFMAN, P. G. 1965 The lift on a small sphere in a shear flow. *J. Fluid Mech.* **22,** 385–400.

SHUEN, J.-S., SOLOMON, A. S. P., ZHANG, Q.-F. & FAETH, G. M. 1985 Structure of particle-laden jets: measurements and predictions. *AIAA Jl* **23,** 396–404.

SNYDER, W. H. & LUMLEY, J. L. 1971 Some measurements of particle velocity autocorrelation functions in a turbulent flow. *J. Fluid Mech.* **48,** 41–71.

SOMMERFELD, M. 1990a Numerical simulation of the particle dispersion in turbulent flows including particle lift forces and different particle/wall collision models. In *Numerical Methods for Multiphase Flows* (Edited by CELIK, I., HUGHES, D., CROWE, C. T. & LANKFORD, D.); *ASME FED* **91,** 11–18. ASME, New York.

SOMMERFELD, M. 1990b Particle dispersion in turbulent flow: the effect of particle size distribution. *Particles Particle Syst. Charact.* **7,** 209–220.

SOMMERFELD, M. & ZEISEL, H. (Eds) 1988 *Proc. 4th Wkshp on Two-phase Flow Predictions, University of Erlangen, March 1987. Bilateral Seminars of the International Bureau.* KFA Jülich, Germany.

TABAKOFF, W. & HAMED, A. 1977 Aerodynamic effects on erosion in turbomachinery. In *Proc. Tokyo Joint Gas Turbine Congr.*, pp. 574–580.

TSUJI, Y., OSHIMA, T. & MORIKAWA, Y. 1985 Numerical simulation of pneumatic conveying in a horizontal pipe. *KONA* **3,** 38–51.

TSUJI, Y., MORIKAWA, Y., TANAKA, T., NAKATSUKASA, N. & NAKATANI, M. 1987 Numerical simulation of gas–solid two-phase flow in a two-dimensional horizontal channel. *Int. J. Multiphase Flow* **13,** 671–684.

YAMAMOTO, F. 1986 A study of motion of a sphere in air flow through horizontal pipe. *Bull. JSME* **29,** 2055–2061.